

Text-guided Generation of Efficient Personalized Inspection Plans

Xingpeng Sun¹, Zherong Pan², Xifeng Gao², Kui Wu², Aniket Bera¹

Abstract— We propose a training-free, Vision-Language Model (VLM)-guided approach for efficiently generating trajectories to facilitate target inspection planning based on text descriptions. Unlike existing Vision-and-Language Navigation (VLN) methods designed for general agents in unknown environments, our approach specifically targets the efficient inspection of known scenes, with widespread applications in fields such as medical, marine, and civil engineering. Leveraging VLMs, our method first extracts points of interest (POIs) from the text description, then identifies a set of waypoints from which POIs are both salient and align with the spatial constraints defined in the prompt. Next, we interact with the VLM to iteratively refine the trajectory, preserving the visibility and prominence of the POIs. Further, we solve a Traveling Salesman Problem (TSP) to find the most efficient visitation order that satisfies the order constraint implied in the text description. Finally, we apply trajectory optimization to generate smooth, executable inspection paths for aerial and underwater vehicles. We have evaluated our method across a series of both handcrafted and real-world scanned environments. The results demonstrate that our approach effectively generates inspection planning trajectories that adhere to user instructions.

I. INTRODUCTION

Inspection planning is a crucial component of autonomous robotic systems tasked with monitoring and assessing known environments. This problem has a wide range of applications, including fault detection in mechanical parts [29], underwater surveying of shipwrecks [3], and structural inspections in civil engineering [4]. In these scenarios, the objective is for an aerial or ground vehicle to efficiently inspect a set of points of interest (POIs). Over the past decade, various methods for coverage and inspection planning have been proposed [2], [10], [6]. However, POIs in inspection planning typically need to be manually defined, either as waypoints or topological constraints, requiring domain-specific knowledge. This dependence can limit the accessibility and adaptability of these methods for non-expert users or in complex environments. Recently, learning-assisted trajectory generation has emerged as a promising solution. These methods automatically convert high-level instructions into low-level inputs, with notable approaches including vision-based target recognition and tracking algorithms [38], [32]. While these algorithms can autonomously generate tracking or goal-reaching trajectories, they often rely on domain-specific vision models. Adapting these models to new domains typically requires data-intensive retraining or a complete algorithm redesign. Although some vision models, such as YOLO [30], can perform open-domain object detection from a single image, they lack the ability to reason across multiple views or infer spatial relationships between camera poses and the observed content.

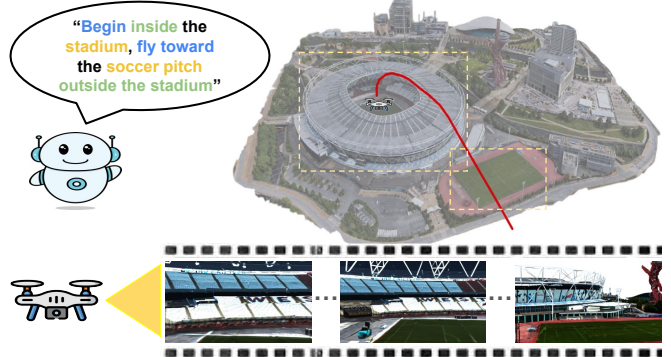


Fig. 1: Our method generates target inspection planning trajectory (red) that conforms to the text description (top left). The text description contains a set of POIs (dashed yellow boxes), the relative robot poses required to observe these POIs (green), the desired visitation order of POIs (blue), and the bottom images show these locations in the first person.

This limitation highlights the need for intuitive, high-level interfaces that bridge human intent with low-level trajectory generation. Recent advancements in open-domain vision-language models (VLMs) offer a promising solution, as they can ground natural language descriptions in visual context, enabling robots to generate inspection trajectories directly from user-provided text prompts.

The latest success of Vision-Language Models (VLMs) has sparked significant interest in using text and visual inputs to guide robotic trajectory generation. Specifically, the Vision-and-Language Navigation (VLN) paradigm enables agents to explore unknown environments by following intuitive, high-level instructions [12], [35]. A key strength of pre-trained VLMs is their strong reasoning capabilities and ability to interpret navigation commands without requiring task-specific fine-tuning [41], thus significantly reducing the need for data-intensive retraining or complete algorithm redesigns. However, while VLN holds promise, these methods typically assume that the agent is environment-agnostic and needs to identify POIs through exploration. In contrast, inspection planning involves environments that are already known, with the primary goal being for the agent to reach a set of predefined POIs as efficiently as possible. Inspection is often performed by aerial or underwater vehicles with limited battery life, further emphasizing the need for efficient trajectory planning. A recent attempt to adapt VLN for UAV trajectory generation [21] marks progress toward this goal but does not leverage VLMs and relies on costly data collection and training procedures. In conclusion, a text-guided, VLM-based trajectory generation approach specifically designed for inspection planning remains a significant and unresolved research challenge.

¹ Purdue University, USA. ² LightSpeed Studios, USA.

Main Results: As illustrated in Figure 1, we propose the first training-free VLM-guided inspection planning algorithm for robot agents equipped with RGB camera sensors to inspect a series of POIs within given environments. The input to our algorithm consists of a 3D environmental map and a general text description that specifies the goal of a personalized inspection plan. This includes the set of POIs, the relative robot poses required to observe these POIs, and the desired order of POI visitation. To generate an inspection plan that aligns with the text description, our method is divided into three stages. First, we construct a Probabilistic RoadMap (PRM), where the nodes represent a set of sampled observation positions. Next, we interact with the VLM to select a subset of nodes from which all POIs are visible from the desired robot poses. Finally, we solve a Traveling Salesman Problem (TSP) to determine the optimal visitation order of the POIs and perform trajectory optimization to compute a smooth and executable robot trajectory. We evaluated our method across both handcrafted meshes and 3D scans of real-world environments. The results demonstrate that our approach can consistently generate trajectories that meet both the text description and the inspection-specific requirements, such as relative robot poses, trajectory smoothness, and/or time-optimality.

II. RELATED WORK

We review representative related works on inspection planning and LLM-guided motion planning.

a) Inspection Planning: Early inspection planning pipelines decompose the task into two main steps: (i) selecting waypoints that collectively observe the set of POIs and (ii) generating a trajectory that passes through all waypoints while ensuring collision avoidance. Minimal-viewpoint solutions, based on Art-Gallery Problem [7] and set-cover heuristics, provide coverage but do not guarantee an optimal overall plan. Thus, subsequent work has turned to variants of TSP [9], trajectory optimization [6], or iterative (re-)sampling of viewpoints to enhance path quality [5]. More recent methods [15], [1] leverage asymptotically optimal, sampling-based motion planners to couple viewpoint selection with trajectory generation. These approaches yield solutions whose cost converges to the optimum as the number of samples increases, albeit at a significant computational cost [11], [16]. However, all of these methods require users to manually specify the set of POIs, limiting the ability to define tasks through more intuitive, high-level specifications such as text descriptions. Motivated by the rise of VLMs, we introduce the first inspection planning framework that accepts free-form text commands. We use a VLM to localize semantic POIs and then invoke trajectory optimization to create a user-friendly, end-to-end inspection planning pipeline. The open-domain nature of VLMs further enables us to incorporate personalized constraints, such as relative robot poses for observing POIs and desired POI visitation orders, making the system more adaptable and intuitive.

b) LLM-guided Motion Planning: The success of pre-trained open-domain VLMs [28], [23] has significantly

boosted the zero-shot performance of data-driven robotic systems in tasks such as table-top manipulation [19], navigation [12], [41], [27], [36], and pick-and-drop operations [20]. These advancements reduce the high costs associated with data collection and fine-tuning when transferring to new problem domains. Recent results further confirm that Large Language Models (LLMs) can generate both coarse- and fine-grained motion plans [19], [17]. In particular, Hong et al. [14] demonstrated that multi-view images can help LLMs understand the 3D world, enabling them to perform navigation tasks. These findings suggest that LLMs are capable of directly generating detailed robot agent inspection trajectories from text descriptions. However, to the best of our knowledge, no existing work has leveraged VLMs specifically for inspection planning. One related effort, AerialVNL [21], trained a VLN model using expert aerial agent trajectory data and crowd-sourced text annotations. However, their training data was not designed for inspection planning tasks. In contrast, our goal is to develop a zero-shot inspection planning system guided by open-domain VLMs, e.g., GPT-4 and DALL-E 3.

III. PROBLEM STATEMENT & METHOD

The input to our method is a known 3D environmental map, denoted by \mathcal{M} , represented using either a mesh or a point cloud, as well as a user-specified text description, as illustrated in Figure 2, which contains a set of POIs and optionally the relative robot poses for observing these POIs, as well as the POI visitation order. The output of our method is the position trajectory $\tau_p(t) : [0, T] \mapsto \mathbb{R}^3$ of an aerial or ground vehicle, with T being the travel time. Our output trajectory not only respects the constraints specified by the text description, but is also efficient to execute with sufficient trajectory smoothness [22], [34]. We design a three-stage pipeline to automatically generate such trajectories guided by a VLM. As our main point of departure from prior works on VLN [12] using sequential decision-making, our method needs to generate and optimize the entire trajectory all at once for efficient execution. Therefore, during our first stage, we extract the POIs and additional constraints by prompting the VLM. We then construct a PRM and detect the set of waypoints for observing each POI. During the second stage, we initialize and iteratively optimize the PRM-restricted trajectory for better smoothness under the constraint that the trajectory always conforms to the text description. Finally, we optimize a continuous trajectory using PRM nodes as waypoints to ensure efficient execution.

A. Stage I: POI Extraction on PRM

We assume that “*The text description consists of a set of POIs, with optional relative robot poses and visitation order constraints.*” Based on this assumption, we use the prompt shown in Figure 2b to extract two sets of POI descriptions, denoted as $\mathcal{L}^o \triangleq \{n_1, n_2, \dots, n_{L^o}\}$ and $\mathcal{L}^u \triangleq \{n_{L^o+1}, n_{L^o+2}, \dots, n_{L^o+L^u}\}$. Here the first set \mathcal{L}^o is an ordered set of L^o POIs, in which the POIs must be visited in the specified order. The second set \mathcal{L}^u is an unordered

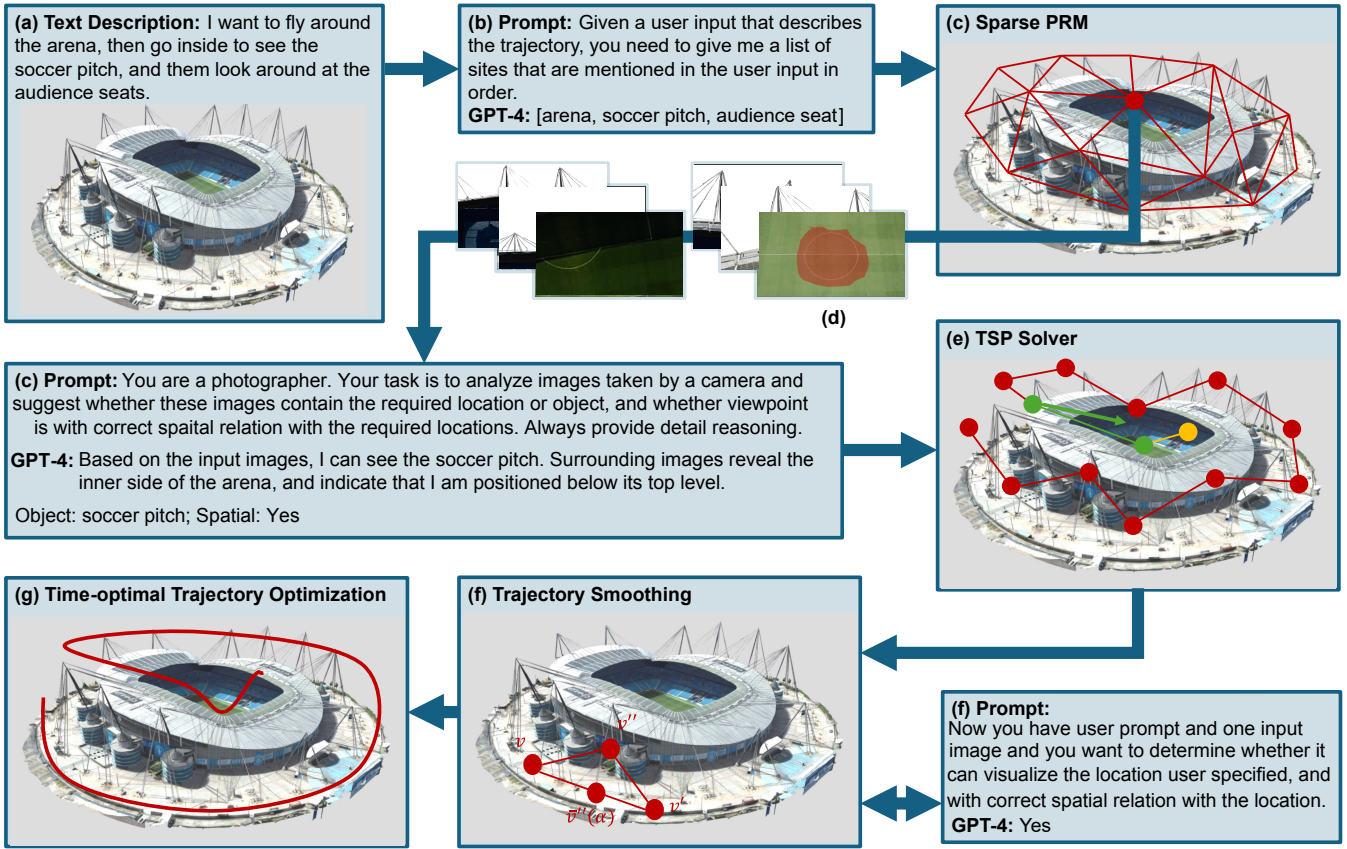


Fig. 2: The pipeline of our method. The input to our method is a text description and a 3D environmental map (a). Our method would first interact with VLM to extract a set of POIs \mathcal{L} (b). Next, we construct a PRM and query each PRM node v from which the POI n_i is visible and salient, while also ensuring that the node satisfies optionally specified robot poses (c). We further ask the VLM to output a pixel-wise segmentation mask of n_i from v , and treat the mass-center of the mask as the desired camera orientation focusing on n_i (d). Next, we compute an initial trajectory connecting all the valid PRM nodes by solving a variant of TSP problems while preserving the optional visitation order of POIs (e), where different color indicates different POIs and the green arrow is the desired camera orientation. After the TSP problem provides an initial trajectory, we interact with VLM for iterative waypoint smoothing (f). Finally, we solve a continuous trajectory optimization, yielding the output (g).

set of L^u POIs, in which the POIs must be visited but the order is arbitrary. Each POI n_i is represented as a pair of text descriptions, i.e., $n_i = \langle \text{name}_i, \text{pose}_i \rangle$, where name_i is the name of POI and pose_i is the optionally user-specified relative pose for the robot to observe the POI. In this work, we pre-specify the following set of possible spatial relations—{inside, over, in-front, around, arbitrary}—where pose_i is labeled as arbitrary if user did not specify any desired spatial relation. In-context examples are appended using the chain-of-thought technique [39] to mitigate VLM hallucination. Thanks to the reasoning capabilities of state-of-the-art VLMs, arbitrary user instructions can be processed.

For each POI n_i , we need to identify a set of inspection positions from which n_i can be clearly observed. To this end, we construct a PRM for the free space of \mathcal{M} . Since naïve PRMs contain many nearby nodes with redundant visual information, leading to excessive VLM queries, we follow [26] and apply Poisson disk sampling. We first sample collision-free points, then sparsify them using Poisson disk sampling, such that the minimal distance between neighboring nodes is at least 10% of the bounding box size of \mathcal{M} . The resulting PRM is a graph $\mathcal{G} \triangleq (\mathcal{V}, \mathcal{E})$ with node set \mathcal{V} and edge set \mathcal{E} . From each PRM node $v \in \mathcal{V}$, we capture six photos of the environment \mathcal{M} from axis-aligned orientations

$(\pm X, \pm Y, \pm Z)$, collecting $6|\mathcal{V}|$ images. For each node, we prompt the VLM to evaluate whether any POI n_i is visible from v and whether the spatial relationship pose_i is satisfied from v . To prompt the VLM, only the user prompt, multi-view images, and in-context examples (image-text pairs with chain-of-thought reasoning) are provided; no 3D model or camera poses are given. A potential pitfall of our approach is that VLM can only evaluate the visibility of a POI, but it is less capable of evaluating the POI saliency. To evaluate saliency, we propose to use an open-domain object segmentation model, GroundedSAM [31], which would predict the segmentation mask of a POI from an image, as well as the Intersection over Union (IoU) score that approximately quantifies object saliency. Combining both open-domain model, we define the saliency indicator $\mathbb{I}_{\text{salient}}(n_i, v)$ where $\mathbb{I}_{\text{salient}}(n_i, v) = 1$ if and only if the IoU of n_i from any of the 6 images taken from v is larger than 0.5 and the VLM confirms that n_i is visible from v and v satisfies the specified pose_i , as shown in Figure 3. If a photo contains multiple POIs, we simply duplicate the PRM node to generate exactly one node clone for each POI. After this procedure, we identify a set of potential waypoints for each n_i denoted as $\mathcal{V}(n_i) = \{v \in \mathcal{V} | \mathbb{I}_{\text{salient}}(n_i, v) = 1\}$, ensuring the inspection trajectory aligns with open-vocabulary user commands.



Fig. 3: A heatmap visualization of the VLM’s spatial understanding of the instruction “*fly inside the stadium*,” where red and green indicates areas considered by VLM to be outside and inside the stadium, respectively. Six images are taken at every sample point and forwarded to the VLM. The six images from the two example views are shown on the top and bottom.

B. Stage II: PRM-restricted Trajectory Generation

We define a PRM node v as valid if $v \in \mathcal{V}(n_i)$ for any n_i , and the set of valid nodes is denoted as $\mathcal{V} \subseteq \mathcal{V}$. Note that the valid node set associated with different n_i is also different due to node duplication. We insert an edge of length zero between a node and its duplications. For any pair of valid nodes v and v' , their distance restricted to the PRM graph is $d(v, v')$. Specifically, we run the Dijkstra algorithm on the PRM graph to calculate the shortest path distance $d(v, v')$ for any $v, v' \in \mathcal{V}$. Our first step is to select an as-smooth-as-possible trajectory restricted to the PRM graph such that each valid node is visited. We further require that the nodes are visited in the order specified in \mathcal{L}_o . In other words, for $i < j \leq L_o$, we ensure that nodes $v \in \mathcal{V}(n_i)$ appear before nodes $v' \in \mathcal{V}(n_j)$. Such a problem can be solved using an extension of TSP with additional order constraints. We formulate and solve such variant TSPs using Miller-Tucker-Zemlin (MTZ) method [8] to cast it as a mixed integer programming (MIP) as illustrated in Figure 2e. Specifically, we define binary auxiliary variable $x_{v \rightarrow v'} \in \{0, 1\}$, which takes value 1 to indicate that the trajectory moves from v to v' . Further, we define binary auxiliary variable $z_v \in \{0, 1\}$ to indicate whether $v \in \mathcal{V}$ is selected or not. We then solve the following mixed integer programming:

$$\min_{y_v \in [1, |\mathcal{V}|-1], x_{v \rightarrow v'} \in \{0, 1\}, z_v \in \{0, 1\}} \sum_v \sum_{v' \neq v} d(v, v') x_{v \rightarrow v'} \quad (1)$$

$$\text{s.t. } \sum_{v \in \mathcal{V}(n_i)} z_v \geq 1, \quad \forall n_i, \quad (2)$$

$$\sum_{v' \neq v} x_{v \rightarrow v'} = z_v, \quad \forall v, \quad (3)$$

$$\sum_{v \neq v'} x_{v \rightarrow v'} = z_{v'}, \quad \forall v', \quad (4)$$

$$y_{v'} - y_v \leq -1, \quad \forall v \in \mathcal{V}(n_i), v' \in \mathcal{V}(n_j), i < j \leq L_o, \quad (5)$$

$$y_{v'} - y_v + |\mathcal{V}| x_{v \rightarrow v'} \leq |\mathcal{V}| - 1, \quad \forall v \neq v'. \quad (6)$$

The objective of the above MIP is to minimize the total travel distance, approximately maximizing smoothness. The first constraint ensures that there is at least one node observing each POI. The second and third constraints ensure that each selected node, as indicated by z_v , is visited exactly once, with one incoming and outgoing edge. The forth and fifth constraints ensure that the generated trajectory is connected and satisfies the specified visitation order constraint.

Specifically, we introduce a continuous variable y_v indicating the visitation order. The forth constraint ensures that, for a pair of nodes v, v' observing two POIs n_i, n_j with $i < j < L_o$, n_j is visited later in the trajectory. The fifth constraint is the MTZ constraint, which ensures the trajectory is connected. Specifically, y_v can be interpreted as the amount of objects stored in node v . The constraint ensures the robot agent removes one object when it visits each node. By restricting all y_v in the range $[1, |\mathcal{V}|-1]$, we essentially avoid disconnected trajectories. Finally, note that we do not care which valid node to visit first, so we introduce a dummy valid node as the first node, which is removed after the TSP solver. After this step, we arrive at an initial trajectory containing a set of waypoints $v \in \mathcal{V}$. There can be other nodes v'' used by the Dijkstra algorithm to connect nodes in \mathcal{V} .

The trajectory created by solving TSP can be rather wiggly and inefficient for robot agent to execute. This is due to the sparse nature of PRM and POI constraints. To resolve this problem, we are inspired by the Frank-Wolfe algorithm [25] and propose an iterative VLM-guided trajectory smoothing scheme. We first use brute-force trajectory simplification, replacing the PRM-restricted trajectory with a straight line, as long as the straight line has no collisions. Then, we check all the nodes v'' in between two nodes v and v' , and try to smooth the trajectory by replacing v'' with the midpoint $\bar{v}'' = (v + v')/2$ (Figure 2f). By iteratively performing such smoothing for each pair of adjacent nodes, the trajectory would contract to a straight line. However, we still need waypoint $v'' \in \mathcal{V}(n_i)$ to observe the POI n_i under consideration, and we need the POI to be visible with a high saliency after moving v'' to \bar{v}'' . We achieve this by interacting with VLM using the prompt illustrated in Figure 2f. As long as VLM confirms that the saliency and the spatial relation constraints are preserved and we check that moving the node will not cause any collisions with \mathcal{M} , we can move v'' to \bar{v}'' . Otherwise, we use a procedure similar to the back-tracing line search during optimization. Specifically, we maintain a search step α and consider moving v'' to $\bar{v}''(\alpha) = \alpha \bar{v}'' + (1 - \alpha)v''$. We will iteratively query VLM at $\bar{v}''(\alpha)$. If the VLM confirms the saliency and spatial constraints are both preserved, we move v'' to $\bar{v}''(\alpha)$. Otherwise, we set $\alpha \leftarrow \alpha/2$ and query again. This procedure is terminated until $\alpha < \underline{\alpha} = 1/8$. Note that for nodes $v \notin \mathcal{V}$, they are just used to connect other nodes and we can simply set them to midpoints without querying VLM. The above smoothing procedure is conducted until no new nodes can be further smoothed. Note that our procedure can be considered as an instance of constrained optimization, with VLM serving as the constraint checker. Intuitively, this procedure can involve a large number of VLM interactions and become the inference bottleneck. To slightly alleviate the inference cost, we order the nodes by their curvature (the angle between the edges $v'' - v$ and $v'' - v'$) and consider the most curved node first. This strategy prevents VLM from repeatedly trying to perform minor improvements using small α . Note this procedure is guaranteed to converge as it monotonically increases the smoothness of the trajectory.

C. Stage III: Continuous Trajectory Generation

The smoothed trajectory from our last section is piecewise linear, which is not efficient for robot execution. Therefore, we design trajectory optimization solver based on [24] to compute a collision-free spline trajectory (Figure 2g). To this end, we first treat the nodes as control points and interpolate a composite Bézier curve. Note that such a Bézier curve might not be collision-free, although the node trajectory is. In this case, we adaptively subdivide the node trajectory so that the interpolated Bézier curve approximates the node trajectory arbitrarily well. We terminate until the Bézier curve is collision-free as well. Next, we solve the collision-free trajectory optimization formulated in [24] that minimizes the integrated snap over the trajectory. We further introduce penalty terms to ensure that all the control points stay as close to the nodes as possible.

After the optimization procedure, all the nodes have been slightly moved because we only use soft penalty constraints to ensure they are close to the original PRM nodes. Therefore, we query the VLM again to extract the segmentation mask of POIs using GroundingSAM and re-focus the camera to the mass-center of the masked regions for each node. Optionally, our method could also output the camera orientation over the entire trajectory by interpolating from the nodes using spherical barycentric coordinates [18]. In other words, at time instance t , the robot position is interpolated from nodes via the stencil:

$$\tau_p(t) = \sum_{j=1}^{d+1} b^j(t) v^j,$$

where v^j is the j th node, $b^j(t)$ is the Bernstein basis coefficient at time t , and d is the order of the curve. Similarly, the camera-orientation is interpolated as:

$$\tau_o(t) = \text{Slerp}(b^1(t), \theta^1, \dots, b^{d+1}(t), \theta^{d+1}),$$

where θ^j is the camera direction, emanating from v^j to the mass-center of the masked region for the POI, and finally $\text{Slerp}(\bullet)$ is the spherical barycentric interpolation function. We summarize our method using the pipeline Algorithm 1.

IV. EVALUATION

In this section, we demonstrate the effectiveness of our methods by evaluating two key aspects of the generated trajectory: *trajectory smoothness*, and *text conformity* that measures the alignment between trajectory and text description. Our implementation is primarily in Python, with trajectory optimization written in C++11. All experiments were conducted on a workstation equipped with a GeForce RTX 3080 GPU. The VLM model used throughout is *GPT-4o* with all parameters set as default. For keypoint extraction, one in-context example is provided in Figure 2b. For spatial relation reasoning, eight in-context examples are used, as shown in Figure 2c, comprising one positive and one negative example for each of the four spatial relations, where each positive example illustrates the correct relation and each negative example depicts a counterexample. For the initial

Algorithm 1 VLM-guided Inspection Trajectory Generation

Require: Text description (2a)

Ensure: τ_p, τ_o

```

1: Extract POI lists  $\mathcal{L}_o$  and  $\mathcal{L}_u$  (Fig. 2b)
2: for each  $v \in \mathcal{V}$  do
3:   for  $i = 1, \dots, L_o + L_u$  do
4:     Compute  $\mathbb{I}_{\text{salient}}(n_i, v)$  (Fig. 2c,2d)
5:   end for
6:   Construct  $\mathcal{V}(n_i)$ 
7: end for
8: Solve MIP to compute initial node list (Fig. 2e)
9: while more nodes can be smoothed do
10:   Order nodes in curvature-descending order
11:   for each consecutive triple  $\langle v, v'', v' \rangle$  do
12:      $\alpha \leftarrow 1$ 
13:     while  $\alpha \geq \underline{\alpha}$  do
14:       if  $v''$  can be moved to  $\bar{v}''(\alpha)$  then
15:          $v'' \leftarrow \bar{v}''(\alpha)$  (Fig. 2f)
16:         break
17:       else
18:          $\alpha \leftarrow \alpha/2$ 
19:       end if
20:     end while
21:   end for
22: end while
23: Solve trajectory optimization for  $\tau_p$  (Fig. 2g)

```

PRM construction, 1000 nodes were sampled. In the Poisson disk sampling step, we ensured the sparsified graph \mathcal{G} was fully connected to guarantee a solution in the subsequent TSP process. In Figure 4, we show four trajectories generated using our method and highlight the key locations identified by VLM, where all the environments come from both scans of the real world and handcrafted meshes. In Figure 5, we show that our pipeline conforms to personalized visitation order. Visually, our trajectory consistently agrees with the input text while being sufficiently smooth for efficient inspection. Below, we conduct more detailed quantitative evaluations.

A. VLM Performance

We evaluate the VLM’s spatial reasoning capabilities based on multi-view images by measuring its winning rate in identifying spatial relationships and processing efficiency. We run 35 samplings for the 6 shown environments and calculate the average rate. To establish ground truth, we manually labeled the bounding boxes of key locations on 3D maps. The VLM’s performance was assessed in determining whether sample points were “*over*”, “*inside*”, “*in front*”, or “*around*” key locations. “*Over*” refers to points positioned on top of the bounding box, while “*inside*” indicates points contained within it. “*In front*” applies to points located in front of the key location, and “*around*” includes points outside the bounding box but still within visible range of the key location. We compare the spatial understanding performance of state-of-the-art VLMs, including GPT-4o, GPT-4o-mini, and the open-source Llama-3.2-11B-Vision, using multi-view

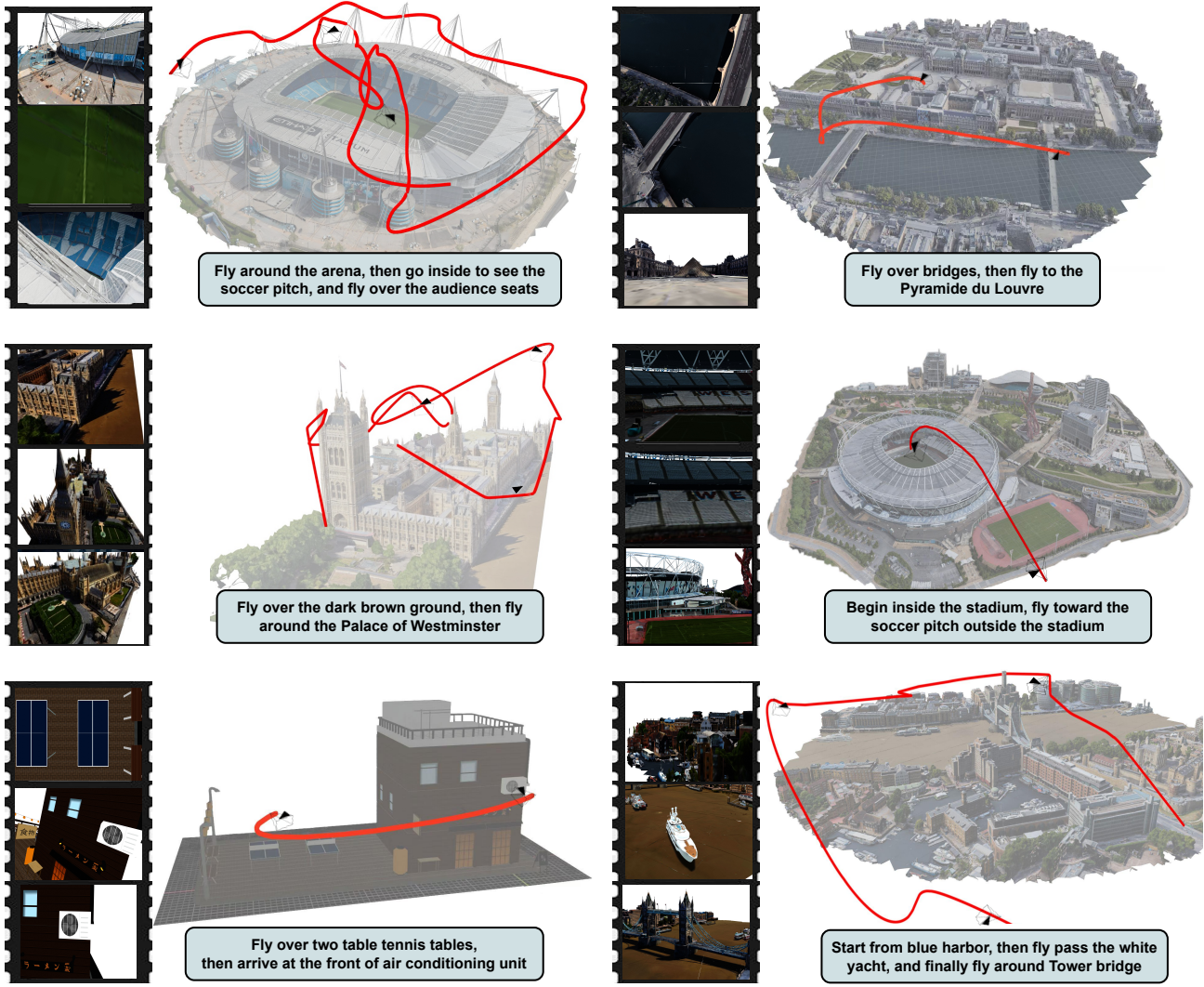


Fig. 4: Outputs of our method, where the inspection trajectories are drawn in red. Robot agent viewpoint camera frames of selected POIs are attached on the left side to highlight text conformity, with the corresponding orientations marked along the trajectory. More visual comparison with previous methods are shown in the supplemental video.

images, as summarized in Table I. Since Llama-3.2-11B-Vision does not natively support multiple image inputs, we concatenate six axis-aligned views into a single composite image before feeding it to the model. GPT-4o achieves over 90% accuracy across all spatial relations, consistently outperforming other models, while Llama-3.2-11B-Vision shows significantly lower accuracy despite longer inference times. We also report the total VLM inference time in III-A and III-B, averaged across all test cases. On average, the VLM reasons over 735 images per scene. Despite the large size of our simulated environments—averaging 520.34k triangles and 305.32k vertices—our method demonstrates efficient performance and operates well within a practical runtime range.

B. Smoothness

The smoothness of the generated trajectory is evaluated using two key metrics: curvature and jerk. In general, lower curvature and jerk value indicate better smoothness of the

TABLE I: VLM Spatial Winning Rate and Inference Time

Model	Time (s)	Winning Rate (%)			Around
		Over	Inside	In front	
GPT-4o	841.32	95.89	90.20	91.93	94.12
GPT-4o-mini	718.47	90.41	86.27	88.71	92.16
Llama-3.2-11B	1166.90	52.83	43.57	40.69	54.48

TABLE II: Comparison of trajectory smoothness, efficiency, and CLIP alignment

Method	κ	Steps	Distance	CLIP	
				ViT-B/32	ViT-B/16
PRM+VLM	0.4834	488.25	47192.89	0.2719	0.2716
LM-Nav[33]	0.4769	87	10544.30	0.2726	0.2714
Ours	0.3865	26.75	2612.85	0.2897	0.2959

trajectory. Curvature, denoted as κ , describes how sharply a curve bends at a particular point. The curvature κ of a trajectory at a point is defined as: $\kappa \triangleq \|\dot{\tau}_p \times \ddot{\tau}_p\| / \|\dot{\tau}_p\|^3$. Here $\dot{\tau}_p$ is the velocity vector and $\ddot{\tau}_p$ is the acceleration vector. Jerk represents the rate of change of acceleration over time

TABLE III: Ablation study on trajectory smoothness

Method	κ	J	steps
Ours	0.3865	0.0036	26.75
-Smoothness	0.4345	0.0053	26.75
Improvement Ratio	12.42%	47.22%	-
-Simplify-Smoothness	0.4646	0.0102	37.67
Improvement Ratio	20.21%	183.33%	40.82%

and indicates the smoothness of motion transitions. For a 3D trajectory, the jerk is defined as the magnitude of the third derivative of the position vector with respect to time t , defined as: $J \triangleq \int_0^T \|\ddot{\tau}_p(t)\| dt$. We further introduce two more metrics, denoted as steps and distance. Steps are defined as the number of line-segment pieces in the PRM-restricted trajectory, i.e., the trajectory before using the trajectory optimization solver in III-C. Distance is defined as the total length of our generated trajectory.

We evaluate our method against two baselines: PRM+VLM and LM-Nav [33]. For PRM+VLM, we construct the Poisson-disk-sampled PRM, use VLM to identify nodes associated with key locations, and then use random node ordering to connect the nodes sequentially. In other words, PRM only uses stage I of our method. LM-Nav [33] is a zero-shot robot navigation technique that generates paths based on high-level text instructions using a topological graph. It is important to note that LM-Nav does not account for spatial constraints, smoothness, and orientation planning, a limitation that our novel approach addresses effectively. We report the average metrics based on the text prompts and mesh environments illustrated in Figure 4, as summarized in Table II. Indeed, our method achieves much better κ , steps, and distance. We further highlight the necessity of our approach using an ablation study in Table III. Here, we compare our method with two simplified versions. For the first version, we remove the VLM-guided smoothing step (-smoothness). For the second version, we remove both the smoothing and path simplification step (-simplify-smoothness), which replaces the PRM-restricted paths with straight lines when possible. Again, our method makes significant improvements over both versions on all three metrics.

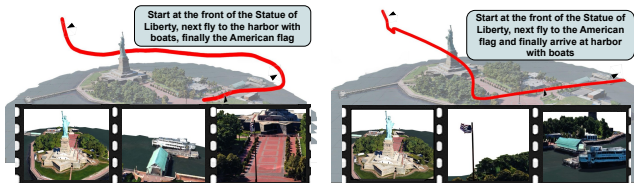


Fig. 5: Results under different visitation order constraints. To follow personalized user text guidance, the left trajectory visits the “harbor with boat” before the “American flag,” while the right trajectory visits the “American flag” first.

C. Text Conformity

The text conformity of the generated trajectory is assessed using the CLIP score [13], which quantifies the alignment between the visual output and the text description of the

trajectory. The CLIP score is defined as:

$$\text{CLIP} = \frac{F_{\text{image}} \cdot F_{\text{text}}}{\|F_{\text{image}}\| \|F_{\text{text}}\|} \in [-1, 1],$$

where F_{image} , and F_{text} are the feature vectors of the image and text produced by the CLIP model, respectively. The CLIP score ranges from -1 to 1, with higher values indicating better conformity to the user-specified locations. For each generated trajectory, we calculate the maximum CLIP score across all camera views on the trajectory relative to each user-specified location provided in the text input. In Table II, we present the average overall maximum CLIP scores under two different CLIP vision transformers [28], ViT-B/32 and ViT-B/16. Our approach is compared with the baseline methods. The CLIP scores are very similar between the three methods. This shows that the additional trajectory smoothing and time-optimal optimization in III-B, III-C did not adversely affect visual satisfaction, i.e., it is capable of smoothing the trajectory while preserving the text conformity. Moreover, re-orienting the camera view towards the mass-center of desired locations potentially enhances visual alignment, resulting in a 0.02 increase in CLIP scores.

V. CONCLUSION & LIMITATIONS

We propose an VLM-guided inspection trajectory generation method from general text descriptions. Our method differs from prior VLN techniques in that it considers the entire trajectory instead of sequentially focusing on the next action. As a result, our method follows a fundamentally different pipeline. We first identify all the POIs and then optimize the trajectory using VLM as a constraint checker. Finally, we solve trajectory optimization to make it efficient to execute. We identify several limitations for further exploration. First, due to the trajectory-wise nature of our operations, our methods need a large number of VLM queries with vision inputs, leading to a high inference cost. In the future, we consider more efficient ways to solve the VLM-constrained trajectory optimization problems. A potential solution is to have VLM generate a constraint that can be handled using conventional numerical optimization [37]. Although we integrate GroundingSAM [31] to assist the VLM in reasoning about visual input, the VLM may still experience hallucinations [40], which can affect our method’s reliability, particularly when it hallucinates and fails to identify a spatial constraint. Fine-tuning the VLM with a large multi-view image dataset is a possible way to improve its spatial relation understanding. Furthermore, due to hardware constraints, we cannot perform 3D large-scale scene reconstruction or real-world navigation. Future work can extend this by conducting real-world experiments.

REFERENCES

- [1] Randa Almadhoun, Tarek Taha, Lakmal Seneviratne, Jorge Dias, and Guowei Cai. A survey on inspecting structures using robotic systems. *International Journal of Advanced Robotic Systems*, 13(6):1729881416663664, 2016.

[2] Elif Ayvali, Hadi Salman, and Howie Choset. Ergodic coverage in constrained environments using stochastic trajectory optimization. In *2017 IEEE/RSJ International Conference on Intelligent Robots and Systems (IROS)*, pages 5204–5210. IEEE, 2017.

[3] Brian Bingham, Brendan Foley, Hanumant Singh, Richard Camilli, Katerina Delaporta, Ryan Eustice, Angelos Mallios, David Mindell, Christopher Roman, and Dimitris Sakellariou. Robotic tools for deep water archaeology: Surveying an ancient shipwreck with an autonomous underwater vehicle. *Journal of Field Robotics*, 27(6):702–717, 2010.

[4] Andreas Bircher, Kostas Alexis, Michael Burri, Philipp Oettershagen, Sammy Omari, Thomas Mantel, and Roland Siegwart. Structural inspection path planning via iterative viewpoint resampling with application to aerial robotics. In *2015 IEEE International Conference on Robotics and Automation (ICRA)*, pages 6423–6430. IEEE, 2015.

[5] Andreas Bircher, Kostas Alexis, Michael Burri, Philipp Oettershagen, Sammy Omari, Thomas Mantel, and Roland Siegwart. Structural inspection path planning via iterative viewpoint resampling with application to aerial robotics. In *2015 IEEE International Conference on Robotics and Automation (ICRA)*, pages 6423–6430, 2015.

[6] Boris Bogaerts, Seppe Sels, Steve Vanlanduit, and Rudi Penne. A gradient-based inspection path optimization approach. *IEEE Robotics and Automation Letters*, 3(3):2646–2653, 2018.

[7] Tim Danner and Lydia E. Kavraki. Randomized planning for short inspection paths. *Proceedings 2000 ICRA. Millennium Conference. IEEE International Conference on Robotics and Automation. Symposia Proceedings (Cat. No.00CH37065)*, 2:971–976 vol.2, 2000.

[8] Martin Desrochers and Gilbert Laporte. Improvements and extensions to the miller-tucker-zemlin subtour elimination constraints. *Operations Research Letters*, 10(1):27–36, 1991.

[9] Stefan Edelkamp, Mihai Pomarlan, and Erion Plaku. Multiregion inspection by combining clustered traveling salesman tours with sampling-based motion planning. *IEEE Robotics and Automation Letters*, 2(2):428–435, 2017.

[10] Mengyu Fu, Oren Salzman, and Ron Alterovitz. Computationally-efficient roadmap-based inspection planning via incremental lazy search. In *2021 IEEE International Conference on Robotics and Automation (ICRA)*, pages 7449–7456. IEEE, 2021.

[11] Jonathan D Gammell and Marlin P Strub. Asymptotically optimal sampling-based motion planning methods. *Annual Review of Control, Robotics, and Autonomous Systems*, 4(1):295–318, 2021.

[12] Jing Gu, Eliana Stefani, Qi Wu, Jesse Thomason, and Xin Eric Wang. Vision-and-language navigation: A survey of tasks, methods, and future directions. *arXiv preprint arXiv:2203.12667*, 2022.

[13] Jack Hessel, Ari Holtzman, Maxwell Forbes, Ronan Le Bras, and Yejin Choi. Clipscore: A reference-free evaluation metric for image captioning. *arXiv preprint arXiv:2104.08718*, 2021.

[14] Yining Hong, Chunru Lin, Yilun Du, Zhenfang Chen, Joshua B Tenenbaum, and Chuang Gan. 3d concept learning and reasoning from multi-view images. In *Proceedings of the IEEE/CVF Conference on Computer Vision and Pattern Recognition*, pages 9202–9212, 2023.

[15] Přemysl Kafka, Jan Faigl, and Petr Váňa. Random inspection tree algorithm in visual inspection with a realistic sensing model and differential constraints. In *2016 IEEE International Conference on Robotics and Automation (ICRA)*, pages 2782–2787, 2016.

[16] Sertac Karaman and Emilio Frazzoli. Sampling-based algorithms for optimal motion planning. *The international journal of robotics research*, 30(7):846–894, 2011.

[17] Teyun Kwon, Norman Di Palo, and Edward Johns. Language models as zero-shot trajectory generators. *IEEE Robotics and Automation Letters*, 2024.

[18] Torsten Langer, Alexander Belyaev, and Hans-Peter Seidel. Spherical barycentric coordinates. In *Symposium on Geometry Processing*, pages 81–88, 2006.

[19] Jacky Liang, Wenlong Huang, Fei Xia, Peng Xu, Karol Hausman, Brian Ichter, Pete Florence, and Andy Zeng. Code as policies: Language model programs for embodied control. In *2023 IEEE International Conference on Robotics and Automation (ICRA)*, pages 9493–9500. IEEE, 2023.

[20] Peiqi Liu, Yawantha Orru, Chris Paxton, Nur Muhammad Mahi Shafiuallah, and Lerrel Pinto. Ok-robot: What really matters in integrating open-knowledge models for robotics. *arXiv preprint arXiv:2401.12202*, 2024.

[21] Shubo Liu, Hongsheng Zhang, Yuankai Qi, Peng Wang, Yanning Zhang, and Qi Wu. Aerialvln: Vision-and-language navigation for uavs. In *Proceedings of the IEEE/CVF International Conference on Computer Vision*, pages 15384–15394, 2023.

[22] Daniel Mellinger and Vijay Kumar. Minimum snap trajectory generation and control for quadrotors. In *2011 IEEE international conference on robotics and automation*, pages 2520–2525. IEEE, 2011.

[23] M Minderer, A Gritsenko, A Stone, M Neumann, D Weissenborn, A Dosovitskiy, A Mahendran, A Arnab, M Dehghani, Z Shen, et al. Simple open-vocabulary object detection with vision transformers. *arXiv preprint arXiv:2205.06230*, 2, 2022.

[24] Ruiqi Ni, Teseo Schneider, Daniele Panozzo, Zherong Pan, and Xifeng Gao. Robust & asymptotically locally optimal uav-trajectory generation based on spline subdivision. In *2021 IEEE International Conference on Robotics and Automation (ICRA)*, pages 7715–7721. IEEE, 2021.

[25] Jorge Nocedal and Stephen J Wright. *Numerical optimization*. Springer, 1999.

[26] Chonhyon Park, Jia Pan, and Dinesh Manocha. Poisson-rrt. In *2014 IEEE International Conference on Robotics and Automation (ICRA)*, pages 4667–4673, 2014.

[27] Lun Quan, Luxin Han, Boyu Zhou, Shaojie Shen, and Fei Gao. Survey of uav motion planning. *IET Cyber-systems and Robotics*, 2(1):14–21, 2020.

[28] Alec Radford, Jong Wook Kim, Chris Hallacy, Aditya Ramesh, Gabriel Goh, Sandhini Agarwal, Girish Sastry, Amanda Askell, Pamela Mishkin, Jack Clark, et al. Learning transferable visual models from natural language supervision. In *International conference on machine learning*, pages 8748–8763. PMLR, 2021.

[29] Roberto Raffaeli, Maura Mengoni, Michele Germani, and Ferruccio Manderli. Off-line view planning for the inspection of mechanical parts. *International Journal on Interactive Design and Manufacturing (IJIDeM)*, 7:1–12, 2013.

[30] Joseph Redmon, Santosh Divvala, Ross Girshick, and Ali Farhadi. You only look once: Unified, real-time object detection. In *Proceedings of the IEEE conference on computer vision and pattern recognition*, pages 779–788, 2016.

[31] Tianhe Ren, Shilong Liu, Ailing Zeng, Jing Lin, Kunchang Li, He Cao, Jiayu Chen, Xinyu Huang, Yukang Chen, Feng Yan, et al. Grounded sam: Assembling open-world models for diverse visual tasks. *arXiv preprint arXiv:2401.14159*, 2024.

[32] Markus Ryll, John Ware, John Carter, and Nick Roy. Semantic trajectory planning for long-distant unmanned aerial vehicle navigation in urban environments. In *2020 IEEE/RSJ International Conference on Intelligent Robots and Systems (IROS)*, pages 1551–1558. IEEE, 2020.

[33] Dhruv Shah, Błażej Osiński, Sergey Levine, et al. Lm-nav: Robotic navigation with large pre-trained models of language, vision, and action. In *Conference on robot learning*, pages 492–504. PMLR, 2023.

[34] Weidong Sun, Gao Tang, and Kris Hauser. Fast uav trajectory optimization using bilevel optimization with analytical gradients. *IEEE Transactions on Robotics*, 37(6):2010–2024, 2021.

[35] Xingpeng Sun, Haoming Meng, Souradip Chakraborty, Amrit Bedi, and Aniket Bera. Beyond text: Utilizing vocal cues to improve decision making in llms for robot navigation tasks. *Transactions on Machine Learning Research*.

[36] Xingpeng Sun, Yiran Zhang, Xindi Tang, Amrit Singh Bedi, and Aniket Bera. Trustnavgpt: Modeling uncertainty to improve trustworthiness of audio-guided llm-based robot navigation. In *2024 IEEE/RSJ International Conference on Intelligent Robots and Systems (IROS)*, pages 8794–8801. IEEE, 2024.

[37] Dimos Tsouros, Hélène Verhaeghe, Serdar Kadioğlu, and Tias Guns. Holy grail 2.0: From natural language to constraint models. *arXiv preprint arXiv:2308.01589*, 2023.

[38] Yuanbin Wang, Minggao Liu, Pai Zheng, Huayong Yang, and Jun Zou. A smart surface inspection system using faster r-cnn in cloud-edge computing environment. *Advanced Engineering Informatics*, 43:101037, 2020.

[39] Jason Wei, Xuezhi Wang, Dale Schuurmans, Maarten Bosma, Fei Xia, Ed Chi, Quoc V Le, Denny Zhou, et al. Chain-of-thought prompting elicits reasoning in large language models. *Advances in neural information processing systems*, 35:24824–24837, 2022.

[40] Ziwei Xu, Sanjay Jain, and Mohan Kankanhalli. Hallucination is inevitable: An innate limitation of large language models. *arXiv preprint arXiv:2401.11817*, 2024.

[41] Gengze Zhou, Yicong Hong, and Qi Wu. Navgpt: Explicit reasoning in vision-and-language navigation with large language models. In *Proceedings of the AAAI Conference on Artificial Intelligence*, volume 38, pages 7641–7649, 2024.